Advances in Materials
2020; 9(3): 42-49
http://www.sciencepublishinggroup.com/j/am
doi: 10.11648/j.am.20200903.11
ISSN: 2327-2503 (Print); ISSN: 2327-252X (Online)

Preparation, Characterization and Catalytic Activity of CrSBA-15 for 2-Propanol Decomposition

M. Sánchez-Cruz[1], R. Hernández-Huesca[1], M. A. Pérez-Cruz[1, *], N. R. Silva-González[2]

[1]Faculty of Chemical Sciences, Autonomous University of Puebla, Puebla, Mexico

[2]Institute of Physics, Autonomous University of Puebla, Puebla, Mexico

Email address:

maria.perezc@correo.buap.mx (M. A. Pére-Cruz)

[*]Corresponding author

To cite this article:

M. Sánchez-Cruz, R. Hernández-Huesca, M. A. Pérez-Cruz, N. R. Silva-González. Preparation, Characterization and Catalytic Activity of CrSBA-15 for 2-Propanol Decomposition. *Advances in materials*. Vol. 9, No. 3, 2020, pp. 42-49. doi: 10.11648/j.am.20200903.11

Received: August 11, 2020; **Accepted**: August 26, 2020; **Published**: September 8, 2020

Abstract: The chromium mesoporous materials have been used in many catalytic reactions. Some studies have been devoted to determining the nature of chromium species and to characterizing the chemical structure. The different chromium species depend on synthetic methods and the support used. In this work we prepared mesoporous SBA-15 supported chromium materials referred to in this document as xCrSBA-15, was prepared by the incipient wetness impregnation method. The materials were characterized by X-ray diffraction (XRD), nitrogen (N_2) adsorption–desorption isotherms, hydrogen temperature-programmed reduction (H_2-TPR), scanning electron microscopic (SEM), energy dispersive X-ray spectroscopy (EDS), diffuse reflectance ultraviolet-visible (UV–vis) and Fourier transform IR (FT-IR). Chromium in SBA-15 forms different types of chromates and Cr_2O_3, causing morphological and textural changes and generating different catalytic centers. The catalytic conversion of 2-propanol to xCrSBA-15 materials were carried out by in a quartz reactor with a loading of 30 mg of the material at 300°C. Before the catalytic test, the material was activated in two ways: with N_2 and reduced at a H_2/Ar flow (MxCrSBA-15). The catalytic conversion of 2-propanol to xCrSBA-15 did not increase with reduction (MxCrSBA-15) but decreased deactivation. All the materials had an acidic behavior, which is related to the chromate species in the materials. These results suggest that the more acidic materials favor the formation of coke during the deactivation process, and coke reduces the Cr^{3+} to Cr^{2+} species, thus decreasing the acidity of the materials.

Keywords: Mesoporous Silica SBA-15, Chromates, Reduced Chromium, 2-Propanol Decomposition

1. Introduction

Porous materials have been intensively studied with regard to technical applications as catalysts and catalyst supports. However, micropore materials such as zeolites cause diffusion limitations when large reactant molecules are involved [1].

The pore size constraints of zeolite materials were addressed by developing mesoporous molecular sieves that have wider pore diameters in the range from 2 to 50 nm, a high surface area (1000-1500 m^2 g^{-1}), uniform framework channels, an excellent sorption capacity (1 cm^3 g^{-1}), etc. [2-4].

On the other hand, mesoporous materials such as SBA-15 possess a high surface area and a suitable wall thickness and pore size for catalytic processes [5]. The most important advantage of these materials is their wall thickness, which is significantly thicker than those of the MCM-type silica [6]. However, these mesoporous materials exhibit a neutral framework, which limits their application in catalytic reactions [7].

Due to the neutral reactivity of the SBA-15 material, several researchers incorporate heteroatoms to its structure, such as Cr [7], Al [8], Fe [9] and Ti [10]. In addition, chromium-containing mesoporous molecular sieves have been studied because of their extensive use in many catalytic reactions [7]. In recent years, supported chromium oxide catalysts have been widely used in dehydrogenation of hydrocarbons [11, 12], selective catalytic reduction of nitrous oxide [13], organic compound oxidation [14, 15], ethylene polymerization, dehydrogenation catalysis [16, 17], hydrogen

production [18] and biodiesel production [19].

Several studies have been devoted to determining the nature of chromium species and to characterizing the chemical structure of the active sites on the catalyst [20]. One method to determine the type and strength of catalytic centers on the materials is the conversion of 2-propanol. This method is often used to test the acid-base properties of the material surface [21]. Two parallel reactions can occur during the process: dehydration to propene mainly on acid sites, and dehydrogenation to acetone on basic or redox sites [22].

Therefore, several studies of 2-propanol decomposition have been carried out in different chromium materials: chromium doped with non-trivalent cations [23], Cr_2O_3/SiO_2 [24], Cr_2O_3 powder [25] and $CrPO_4/AlPO_4$ [26].

Recently, Cuesta Zapata *et al.* [20] reported that, when 2-propanol is decomposed on MCM-41 chromium/silica materials with different hydrothermal treatments, these treatments improved the chromium/silica interaction thorough chromasiloxane ring formation. These anchored Cr^{3+} species developed highly unsaturated Lewis acid sites responsible for the 2-propanol dehydration.

Tredja [27] reported a comparative study of the incorporation of chromium species via incipient wetness impregnation into mesoporous silica of MCM-41 type, SBA-3 and SBA-15, where they found that the formation of active centers on different silica supports strongly depends on the preparation conditions used in their synthesis.

Additionally, various synthetic methods are expected to result in different chromium species and the different chromium species may behave differently in catalytic reactions [28]. Thus, in this work, we have prepared SBA-15 and chromium-supported mesoporous SBA-15 (xCrSBA-15) by the wetness impregnation method. The type and strength of catalytic centers on materials were determined to the conversion of 2-propanol in the non-reduced and reduced materials with H_2 before the reaction.

2. Experimental

2.1. Synthesis of the Materials

The mesoporous silica SBA-15 support was synthesized using sodium silicate as silica source as reported previously by Gómez-Cazalillas *et al.* [29]. The materials were prepared by the incipient wetness impregnation method with Cr $(NO_3)_3 \cdot 9H_2O$ as chromium precursors. The impregnated support was dried at 80°C for 12 h and calcined at 550°C for 5 h, with a ramp of 1°C min^{-1}. These materials were assigned as xCrSBA-15, where x is the weight percentage of metal loading (2, 5 and 10 wt%).

2.2. Characterization

The scanning electron microscopic (SEM) images and EDS analysis were recorded on a JEOL JSM-7800F microscope operated at 30 kV. X-ray powder diffraction patterns were recorded with CuKa radiation on a D8 Discover Bruker diffractometer, operated at 40 kV and 35 mA. XDR data were recorded at a small angle from 2θ in the range from 0.6 to 2° and a wide-angle from 20 to 80°. Nitrogen adsorption isotherms of the materials were made with an Autosorb-1C-MS instrument after materials were outgassed at 200°C for 12 h in vacuum before measurements were made. The surface areas and pore size distribution were determined by BET and BJH methods, respectively. FTIR spectra were collected on a Varian Excalibur spectrometer in the range from 4000 to 400 cm^{-1}, before and after measuring catalytic activity, using 1 mg of materials by 150 mg of KBr. UV-vis spectra of the materials in the range from 200 to 1900 nm were obtained on a UV-vis spectrophotometer Varian-Cary 300 before and after measuring catalytic activity. The reducibility of the materials was determined by H_2 temperature-programmed reduction (H_2-TPR) using 80 mg of the materials in H_2/Ar (10 vol% in Ar) with a heating rate of 10°C min^{-1} from 25 to 600°C. To carry out these measurements, the materials were previously treated with oxygen (flow rate = 60 cm^3 min^{-1}) at 550°C for 4 h.

2.3. Measuring the Catalytic Activity

The reaction of 2-propanol decomposition was carried out in a quartz reactor with a loading of 30 mg of the material. Before the catalytic test, the material was activated in two ways. In the first way, the xCrSBA-15 materials were activated at 300°C for 2 h under N_2 with a flow rate of 60 cm^3 min^{-1} to the materials. In the second way, the materials were reduced at a H_2/Ar flow rate of 100 cm^3 min^{-1} for 2 h at 600°C. Then, the materials were cooled to 300°C under a N_2 flow (60 cm^3 min^{-1}) to the materials. These new materials were called MxCrSBA-15. In the catalytic test, 2-propanol was fed into the reactor through a saturator using N_2 as a carrier gas with a flow rate of 60 cm^3 min^{-1}. The partial pressure of 2-propanol used was 22.4 Torr, and the conversion was studied at 300°C. The products were identified with a Perkin Elmer Autosystem XL gas chromatographer with a flame ionization detector (FID) and a Porapak N column.

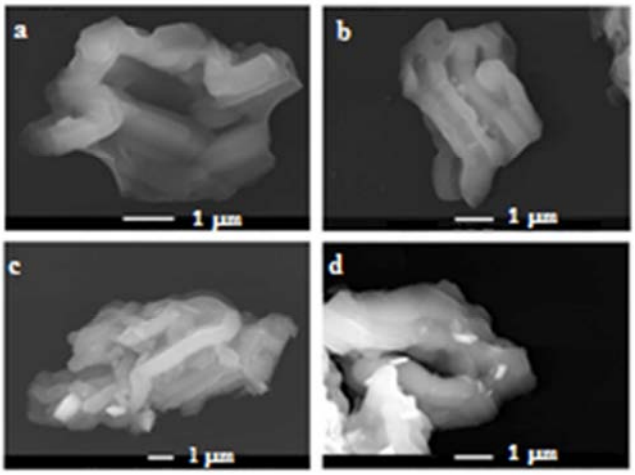

Figure 1. *SEM micrographs of the materials: mesoporous silica support (a) SBA-15 and chromium-supported in mesoporous silica (b) 2CrSBA-15, (c) 5CrSBA-15 and (d) 10CrSBA-15.*

3. Results and Discussion

3.1. Characterization of the Materials

The materials obtained show different colors depending on the amount of chromium, that is, yellow for 2%, green for 5% and dark green for 10% of Cr loading. These colors indicate that there are different Cr species in the materials [30]. The 2CrSBA-15 coloring exhibits the presence of the Cr^{6+} species (chromate or polychromate), due to the rapid oxidation of Cr^{3+} to Cr^{6+} in the nitrate salt solution before being impregnated [31], while the 5CrSBA-15 and 10CrSBA-15 colorings are green, which is a characteristic color indicating the presence of Cr^{3+} species, such as Cr_2O_3 [20].

The estimated percentage of metal present in the xCrSBA-15 materials by an EDS analysis reveals that there is a minimal difference between the experimental concentration on the surface and the theoretical content of chromium (Table 1). These results demonstrate that the incipient wetness impregnation method is efficient in the preparation of these materials.

3.1.1. xCrSBA-15 SEM

The external structure of the xCrSBA-15 materials characterized by SEM is presented in Figure 1. The SBA-15 support (Figure 1a) has a typical long-chain structure, between 200 and 600 nm in diameter, while the 2CrSBA-15 and 5CrSBA-15 materials (Figure 1b and 1c) have a chain-like structure that breaks into separate rod-like sub-units. The 10CrSBA-15 material (Figure 1d) displays the presence of a small rod-like structure that forms irregular spherical particles where pore formations can be observed [32, 33, 34]. The structural change of the xCrSBA-15 materials probably occurs due to a strong interaction between chromium nitrate and silica during the calcination of Cr precursor in oxygen at 550°C. According to Wang *et al.*, while chromium nitrate interacts with the Si—OH of the SBA-15 material to form Si—O—Cr and Cr—O—Cr linkages, these interactions result in the weakening of the Si—O—Si bonds and the breaking of long interconnected chains and the later formation of crystalline α-Cr_2O_3 at elevated chromium loadings [32]. As previously observed, the 5CrSBA-15 and 10CrSBA-15 materials (Figure 1c and 1d) contain needle-shaped and cube-shaped crystalline structures of Cr_2O_3 [35]. This result was confirmed by an X-ray diffraction analysis.

3.1.2. X-ray Diffraction

Figure 2 depicts the patterns of the XRD support and catalytic materials. At the low angle range (Figure 2a), all the materials exhibit an intense diffraction peak at ~1°, which can be indexed as the typical pattern of hexagonal structure attributed to the diffraction plane (1 0 0) [36]. With an increasing Cr content, the intensity of the (1 0 0) peak decreases as a result of a partial blocking of the SBA-15 mesopores and the deterioration of the ordered pore structure [32]. All the materials exhibit significant changes from the *d*-spacing of the (1 0 0) plane to lower values in relation to the SBA-15 material, implying dilation in the framework lattice [37]. It is important to take into consideration that there is a decrease in the unit cell constant (a_0) and the wall thickness (e) in these materials (Table 1). A similar result has also been reported by Charan so the decrease in the a_0 is attributed to a possible disruption in the inter-particle growth mechanisms at a macroscopic scale, which is in agreement with its structural change as it creates an ordered array of spheres [37]. Figure 2b depicts a broad peak at 2θ = 23.2° attributed to SiO_2 (the component of SBA-15) [38]. There are no diffraction peaks assignable to crystalline Cr_2O_3 in the 2CrSBA-15 material. It may be deduced that the chromium species are highly dispersed on the surface of SBA-15 or that the particle size of chromium oxide may be small to be detected by XRD [35]. However, the 5CrSBA-15 and 10CrSBA-15 materials have the same peaks at 2θ = 24.5°, 33.6°, 36.2°, 39.7°, 41.5°, 44.2°, 50.2° and 54.8°, attributable to the hexagonal phase of Cr_2O_3 from the JCPDS powder diffraction file (PDF card 00-038-1479) [39]. The intensity of the Cr_2O_3 peaks grows by increasing the chromium loading [40].

3.1.3. N_2 Adsorption/Desorption Isotherms

The N_2 adsorption-desorption isotherms of the SBA-15 support and the xCrSBA-15 materials are type IV with H1-type hysteresis (Figure 3a). This feature is typical of mesoporous materials with one-dimensional cylindrical channels [36]. The adsorption-desorption isotherms exhibit a hysteresis loop extended to very low relative pressures ($P/P_0 <$ 0.3). This low-pressure hysteresis may be the result of a change in the porous structure of the material, such as a swelling of a non-rigid structure [41, 42]. An X-ray diffraction analysis of the xCrSBA-15 materials confirms the change in the porous structure. The decline on the surface area and pore volume may be the result of the blocking by CrOx in the pores of the SBA-15 support (Table 1) [32]. Regarding the mesopore size distribution (Figure 3b), the support has pores between 30 and 50 Å with an average pore diameter of ~40.5 Å. The materials impregnated with Cr (xCrSBA-15) exhibit a decrease in the intensity of the distribution peak with respect to the SBA-15 peak, which implies a blockage of pores.

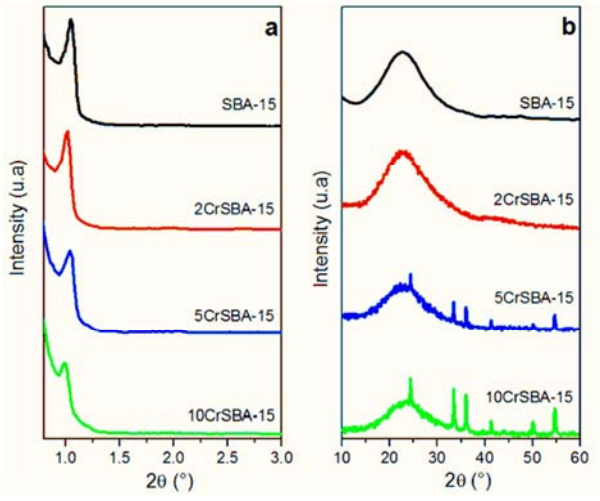

Figure 2. *(a) Low angle and (b) high-angle XRD patterns of the mesoporous silica support SBA-15 and the chromium-supported in mesoporous silica 2CrSBA-15, 5CrSBA-15 and 10CrSBA-15.*

Table 1. *Percentage of metals present in the materials estimated by an EDS analysis and the structural properties of the support and the xCrSBA-15 materials.*

Materials	SBA-15	2CrSBA-15	5CrSBA-15	10CrSBA-15
Metal content (wt%)[a]	–	1.98	4.59	9.20
Planar distance d_{100} (Å)	83.93	86.81	84.21	88.62
Lattice constant a_0 (Å)[b]	167.86	100.23	97.23	102.23
Wall thickness e (Å)[c]	127.36	58.13	155.33	61.43, 66.83
Surface area ($m^2 g^{-1}$)[d]	912.96	419.21	340.67	340.67
Pore volume ($cm^3 g^{-1}$)[e]	0.79	0.47	0.43	0.40
Average pore size (Å)[f]	40.5	42.1	41.9	40.8, 35.4

[a] Calculated by SEM
[b] $a_0 = 2x\, d_{100}/\sqrt{3}$
[c] Calculated by $e = a_0$-pore size
[d] Calculated by BET method
[e] Mesopore volume by BJH
[f] Calculated by BJH method

A slight shift towards larger pores occurs in the distribution peaks of the 2CrSBA-15 and 5CrSBA-15 materials, which may be attributed to a swelling of the mesopores caused by the impregnation of Cr in their walls (r_{aq} of Cr^{3+} = 0.6 Å [43]). This distortion is also observed in the micropores as a consequence of low pressure hysteresis. On the other hand, the 10CrSBA-15 material exhibits a narrower pore distribution found within the SBA-15 distribution peak with two maximums at 40.8 Å and 35.4 Å. This result may be attributed to a change in structure by the presence of Cr_2O_3 [33].

3.1.4. H_2-TPR

Figure 4 depicts the H_2-TPR profiles of the materials supported with Cr (xCrSBA-15), where several H_2 consumption peaks are observed, indicating the presence of various species of Cr in the materials. A poorly defined peak is observed at ~200°C, which may be attributed to the reduction of Cr^{6+} to Cr^{5+}. Similarly, approximately at this temperature CrO_3 is melted and decomposed by deoxygenation to form Cr_2O_3 [44]. A second peak between 280 and 300°C is attributed to the reduction of Cr^{6+} to Cr^{4+} and Cr^{3+}, which was ascribed by Fouad [44] to the formation of $Cr_2(CrO_4)_3$, by thermal decomposition of CrO_3. A peak at ~390°C is observed in the three xCrSBA-15 materials. This H_2 consumption peak has been reported for materials impregnated with Cr by incipient wetness and is related to the reduction of Cr^{6+} species such as mono-, di-, tri- and tetrachromates isolated on the surface of the material. Shi associate this reduction to the presence of soluble Cr^{6+} as suggested by Cavani [12, 45]. Another H_2 consumption peak at ~480°C is observed in 10CrSBA-15, but it cannot be seen in 5CrSBA-15 and it only appears as a small shoulder in 2CrSBA-15, which is attributed to the reduction of Cr^{6+} to Cr^{3+} to form Cr_2O_3 [7, 12, 44]. Finally, a peak at ~543°C is observed in 2CrSBA-15 and 5CrSBA-15 and it appears as a shoulder in 10Cr SBA-15. This peak has been reported for materials produced by adding Cr during the synthesis of the support and is associated to the reduction of ions from Cr^{6+} to Cr^{3+} grafted on the surface of the silica, making it difficult to reduce [12, 27]. Other authors have also attributed it to the reduction of Cr^{3+} to Cr^{2+} during the reduction of CrO_3 [44].

3.2. Conversion of 2-Propanol on xCrSBA-15 and MxCrSBA-15 Materials

Figure 5 compares the conversion of 2-propanol to propene and acetone in the xCrSBA-15 (Figure 5a) and MxCrSBA-15 (Figure 5b) materials, where 5CrSBA-15 exhibits the highest conversion ability. It is observed that all the materials have a higher conversion ability towards propene formation, including the SBA-15 material that has a conversion to propene of less than 4%, but it does not present conversion to acetone. The 2CrSBA-15 material has the lowest conversion ability, whereas the 5CrSBA-15 and 10CrSBA-15 materials have a similar conversion ability to propene and acetone. The high Cr_2O_3 content does not favor conversion. Apparently, the activity of the materials is related to the presence of soluble and grafted chromates [27]. On the other hand, the reduction of these materials (M5CrSBA-15 and M10CrSBA15) does not change the initial conversion, but it inhibits deactivation [46].

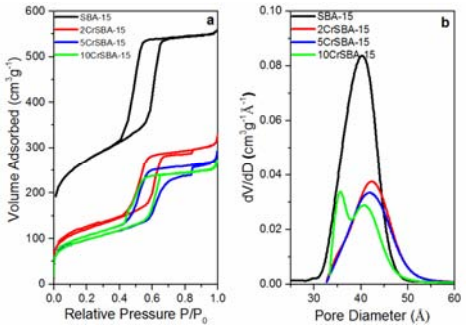

Figure 3. *(a) Adsorption-desorption isotherms and (b) pore size distributions for the mesoporous silica support SBA-15 and the chromium-supported in mesoporous silica 2CrSBA-15, 5CrSBA-15 and 10CrSBA-15.*

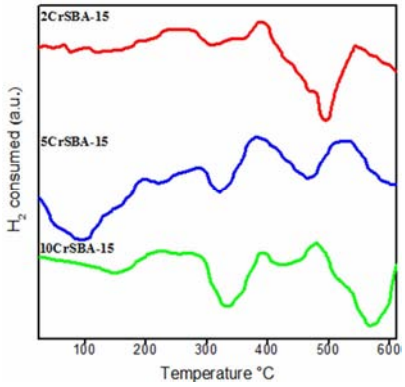

Figure 4. *H_2-TPR profiles of chromium-supported in mesoporous silica 2CrSBA-15, 5CrSBA-15 and 10CrSBA-15.*

The xCrSBA-15 materials present a greater deactivation, thus a greater number of acidic species (Cr^{6+}) or soluble chromates that dehydrate form Cr_2O_3 determined by UV-vis (Figure 7), and they are also more susceptible to carbon poisoning or coke formation [47]

Regarding the selectivity of the materials (Figure 6), the xCrSBA-15 materials increase their selectivity to propene in relation to time (Figure 6a) and the reduced MxCrSBA-15 materials decrease their selectivity after a few minutes (Figure 6b). This phenomenon is the opposite in acetone. The selectivity towards dehydrogenation or dehydration of 2-propanol in the studied materials is explained by the relationship with the Cr species determined by IR and UV.

3.2.1. Uv-vis Spectroscopy of the CrSBA-15 Materials Before and After the 2-Propanol Conversion Reaction

The unused xCrSBA-15 materials have bands that correspond to the Cr^{6+} and Cr^{3+} species (Figure 7). The bands at 260 and 360 nm have been found in silica modified with Cr; they are typical of Cr^{6+} species caused by charge transfer of monochromate species [48].

Another band that corresponds to the dichromate species is observed at 455 nm and increases its intensity with the chromium content due to an increase in the degree of polymerization of the Cr^{6+} species [48]. The band corresponding to the Cr^{3+} species appears at 600 nm and is attributed to the Cr^{3+} species in the α-Cr_2O_3 particles [49-51]. In the spectra of xCrSBA-15 (Figure 7c) and MxCrSBA-15 (Figure 7d) materials after the reaction, the charge transfer bands of the Cr^{6+} species located at 380 and 450 nm are more evidently observed. The band of the d-d transitions of the Cr^{3+} located at ~600 nm increases its intensity, indicating the reduction of CrO_3 to Cr_2O_3 [52, 53]. Only in the MxCrSBA-15 materials is there a band at 324 nm corresponding to the transition from O → Cr^{2+} in the silica [54]. There are also two other bands: the first at ~1000 to 1333 nm, and the second at ~1428 nm (insert) with very low response corresponding to Cr^{2+} pseudo-tetrahedral species. This band is more intense in the MxCrSBA-15 materials [53, 54].

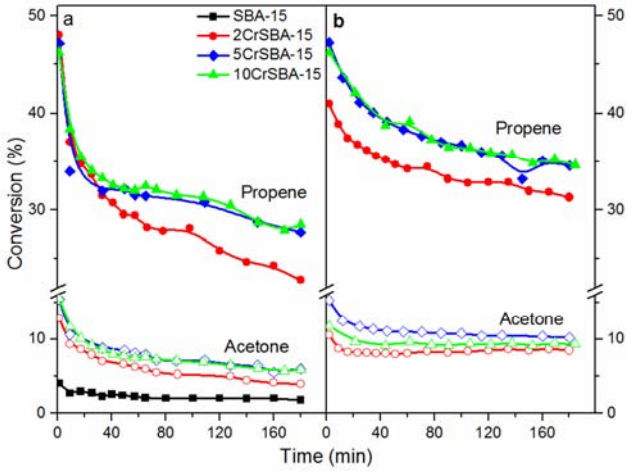

Figure 5. *Conversion of 2-propanol to propene (solid symbol) and acetone (open symbol) on chromium-supported in mesoporous silica materials: (a) non-reduced xCrSBA-15 and (b) reduced MxCrSBA-15 materials.*

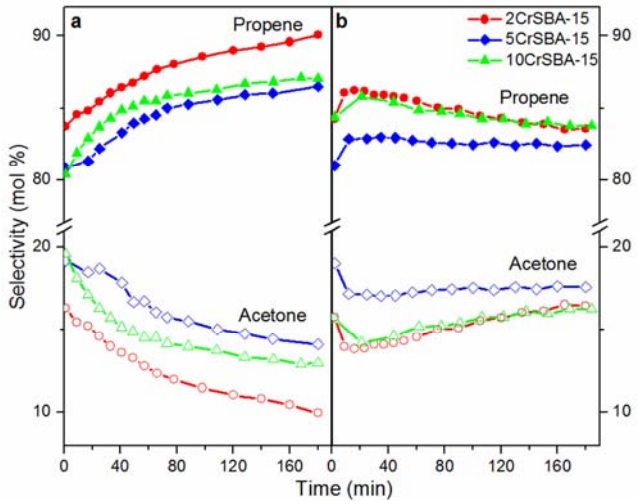

Figure 6. *Selectivity to propene (solid symbol) and acetone (open symbol) on chromium-supported in mesoporous silica materials: (a) non-reduced xCrSBA-15 and (b) reduced MxCrSBA-15 materials.*

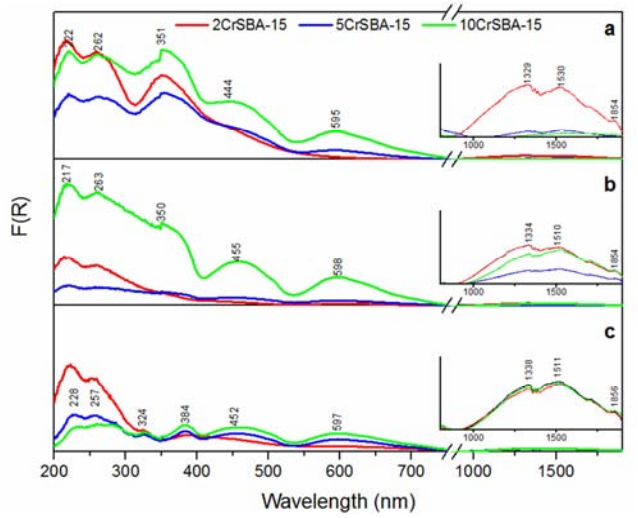

Figure 7. *Diffuse reflectance spectra of (a) the non-used xCrSBA-15, (b) the used non-reduced xCrSBA-15 and (c) the used reduced MxCrSBA-15 materials.*

Table 2. *Percentages of chromium species in the unused xCrSBA-15 materials and the used xCrSBA-15 and MxCrSBA-15 materials after decomposition of 2-propanol.*

Materials	% species			
	Mono- chromate	Di- and polychromate	Cr^{3+}	Cr^{2+}
Unused				
2CrSBA-15	91.0	0.0	0.0	9.04
5CrSBA-15	69.6	21.5	8.1	0.77
10CrSBA-15	64.3	22.0	13.7	0.00
Used				
2CrSBA-15	58.6	11.9	8.1	21.43
5CrSBA-15	39.7	36.2	18.3	5.80
10CrSBA-15	46.4	35.8	15.2	2.51
M2CrSBA-15	44.8	26.5	10.0	18.74
M5CrSBA-15	25.7	36.9	21.5	15.93
M10CrSBA-15	18.8	39.9	26.7	14.70

Considering the area under the curve of the bands of the UV-vis spectra (Table 2), the percentage of the chromium species can be estimated. The results indicate that all the

xCrSBA-15 materials have high percentages of monochromate and dichromate species (Cr^{6+}). However, a decrease in the percentage of Cr^{6+} species is observed in the used xCrSBA-15 and MxCrSBA-15 materials, whereas there is an increase in the percentage of Cr^{3+} and Cr^{2+} species due to the reduction process. The MxCrSBA-15 materials have higher percentages of Cr^{2+}.

3.2.2. FTIR Spectroscopy of the CrSBA-15 Materials Before and After the 2-Propanol Conversion Reaction

In the FTIR spectra of the SBA-15 support and the xCrSBA-15 materials used and unused in the 2-propanol reaction, a band at ~3450 cm^{-1} (not presented here) is observed, which is attributed to the SiOH group on the surface of the SBA-15 support [55]. On the other hand, Figure 8 depicts the spectra of the SBA-15 support and the unused xCrSBA-15 materials. A band at 1636 cm^{-1} is observed corresponding to the bending vibrations of the adsorbed water [57]. There is a slight increase with Cr loading in the band, indicating that Cr is bound to the surface of the silica and is hydrated. A band at 1085 cm^{-1} and a shoulder at 1200 cm^{-1} indicate ν_{as} (Si—O—Si), where there is a decrease in their intensity with the impregnation of Cr [32], while a band at 795 cm^{-1} corresponds to ν_s (Si—O—Si), and a band at 460 cm^{-1} corresponds to the bending group O—Si—O [56], where there is an increase in their intensity. There is a variation in the intensity of all these bands in comparison to the bands of the SBA-15 support. A band that appears at 964 cm^{-1} has generally been assigned to Si—O vibration in Si—OH groups [57]. A shift of this band at 959 cm^{-1} is recorded for the xCrSBA-15 materials, which could be attributed to defects in the Si—O—M stretching modes, where M = Cr [57], due to the presence of chromates on the surface. The bands at 571 and 631 cm^{-1} appear in the spectra of the 5CrSBA-15 and 10CrSBA-15 materials, where the intensity is higher in the latter attributable to vibrations in hydrated Cr_2O_3 on the surface of the pores, as reported by other authors [33, 57, 58]. The materials used in the 2-propanol conversion reaction exhibit a slight shift to higher wavenumbers of the shoulder at 1200 cm^{-1}, which indicates the presence of C—O bonds, whose band appears at 1260-1000 cm^{-1} [22, 55]. The band at 958 cm^{-1} decreases in those materials used in the 2-propanol reaction and almost disappears in the previously reduced materials (MxCrSBA-15). This shift may be attributed to the Cr^{6+} bound as chromate that is reduced to form Cr_2O_3. Similarly, the bands at 571 and 631 cm^{-1} decrease in intensity after the 2-propanol reaction. The change in these bands and the appearance of a small band at 1380 cm^{-1} may be attributed to the formation of C—H bonds that inhibit the activity of the materials [22, 46].

4. Conclusion

Chromium materials of well-ordered mesoporous structure were generated using the incipient wetness impregnation method. These materials contain chromate and Cr_2O_3 in their structure. The results of the catalytic evaluation indicate a high selectivity to the formation of propene due to the presence of chromates on the surface of the materials, which is an evidence of their acidic behavior. Although the high content of chromium causes the formation of chromium oxide, its presence does not improve the catalytic activity of the xCrSBA-15 materials. The reduced materials (MxCrSBA-15) do not increase the conversion of 2-propanol to propene and acetone, but they do become deactivated in relation to time, whereas the non-reduced materials (xCrSBA-15) do increase their selectivity to propene in relation to time due to a self-reduction of chromate ions.

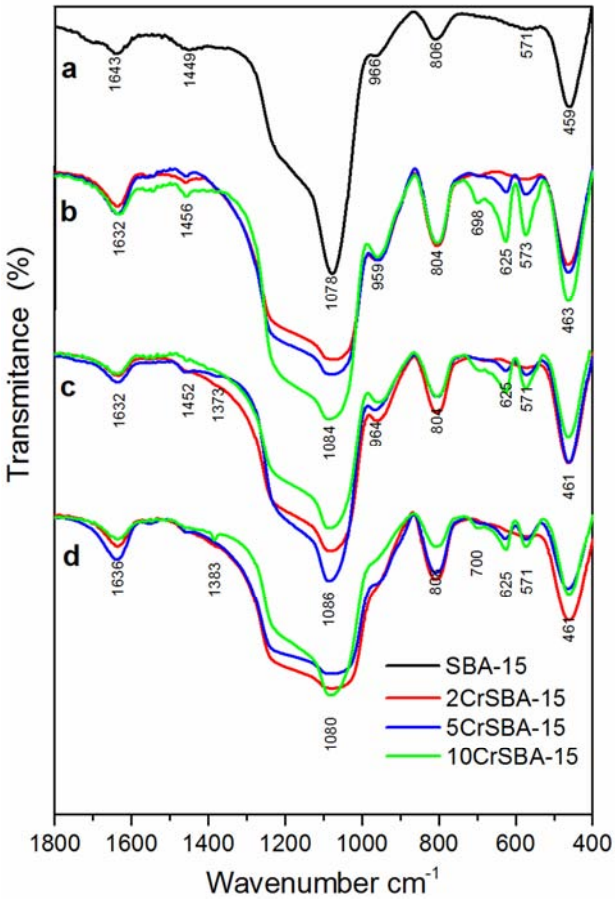

Figure 8. *FTIR spectra of (a) the SBA-15, (b) the non-used xCrSBA-15, (c) the used non-reduced xCrSBA-15 and (d) the used reduced MxCrSBA-15 materials.*

Acknowledgements

The authors are grateful to National Council for Science and Technology (CONACyT, Mexico) for the financial support through Scholarship No. 257187 and to Vice-rectory for Research and Graduate Studies (VIEP) Project 00241.

References

[1] Taguchi, A. and F. Schüth (2005). Ordered mesoporous materials in catalysis. Microporous Mesoporous Materials, 77: 1-45 (2005).

[2] Pastore, H. O., Coluccia, S., Marchese, L. (2005). Porous Aluminophosphates: From Molecular Sieves to Designed Acid Catalysts. Annual Review of Materials Research, 35: 351-395.

[3] Chen, S. Y., Tang, C. Y., Chuang, W. T., Lee, J. J., Tsai, Y. L., Chan, J. C. C., Lin, C. Y., Liu, Y. C. and Cheng, S. (2008). A Facile Route to Synthesizing Functionalized Mesoporous SBA-15 Materials with Platelet Morphology and Short Mesochannels. Chemistry Materials 20 (12): 3906-3916.

[4] Wu, Z. and Zhao, D. (2011). Ordered Mesoporous Materials as Adsorbents. Chemical Communications, 47: 3332-3338.

[5] Zhao, D., Sun, J., Li, Q. and Stucky, G. D. (2000). Morphological control of highly ordered mesoporous silica SBA-15. Chemistry of Materials, 12: 275–279.

[6] Kuśtrowski, P., Chmielarz, L., Dziembaj, R., Cool, P. and Vansant, E. F. (2005). Modification of MCM-48-, SBA-15-, MCF-, and MSU-type Mesoporous Silicas with Transition Metal Oxides Using the Molecular Designed Dispersion Method. Journal of Physical Chemistry B, 109 (23): 11552-11558.

[7] Zhao, X. and Wang, X. (2007). Synthesis, characterization and catalytic application of Cr–SBA-1 mesoporous molecular sieves. Journal of Molecular Catalysis A: Chemical, 261 (2): 225-231.

[8] Gallo, J. M. R., Bisio, C., Gatti, G., Marchese, L. and Pastore, L. O. H. (2010). Physicochemical characterization and surface acid properties of mesoporous Al-SBA-15 obtained by direct synthesis. Langmuir, 26: 5791–5800.

[9] Lei, Z. B., Bai, S. Y., Dang, L. Q., Xia H. A., Xu, Q., Cao, Y. D., An, L. Z., Zhao, M. Y., Lo, A. Y. and Liu, S. B. (2009). Fe_2O_3/SBA-15 catalyst synthesized by chemical vapor infiltration for Friedel–Crafts alkylation reaction. Microporous Mesoporous Materials, 123, 306–313.

[10] Zhu, S. M., Zhang, D., Zhang, X. C., Zhang, L., Ma, X. W., Zhang, Y. L. and Cai, M. (2009). Sonochemical incorporation of nanosized TiO_2 inside mesoporous silica with high photocatalytic performance. Microporous Mesoporous Materials, 126: 20–25.

[11] Weckhuysen, B. M., Wachs, I. E. and R. A. Schoonheydt, R. A. (1996). Surface Chemistry and Spectroscopy of Chromium in Inorganic Oxides. Chemical Reviews, 96: 3327-3350.

[12] Shi, X., Ji, S. and Wang, K. (2008). Oxidative dehydrogenation of ethane to ethylene with carbon dioxide over Cr–Ce/SBA-15 catalysts. Catalysis Letters, 125: 331-339.

[13] Chmielarz, L., Kuśtrowski, P., Kruszec, M., Dziembaj, R., Cool, E. F and Vansant, J. (2005). Nitrous oxide reduction with ammonia and methane over mesoporous silica materials modified with transition metal oxides. Journal of Porous Materials, 12: 183-191.

[14] Zhang, W. and Pinnavaia, T. J. (1996). Transition metal substituted derivatives of cubic MCM-48 mesoporous molecular sieves. Catalysis Letters, 38: 261-265.

[15] Shylesh, S., Samuel, P. P. and Singh, A. P. (2007). Chromium-containing small pore mesoporous silicas: Synthesis, characterization and catalytic behavior in the liquid phase oxidation of cyclohexane. Applied Catalysis A: General, 318: 128-136.

[16] McDaniel, M. P. (1981). The state of Cr (VI) on the Cr/Silica polymerization catalyst. Journal of Catalysis, 67 (1): 71-76.

[17] Zhang, X., Yue, Y. and Gao, Z. (2002). Chromium oxide supported on mesoporous SBA-15 as propane dehydrogenation and oxidative dehydrogenation catalysts. Catalysis Letters, 83, 19-25.

[18] Calles, J. A., Carrero, A., Vizcaíno, A. J. and P. J. Megía P. J. (2018). Agglomerated Co-Cr/SBA-15 catalysts for hydrogen production trought acetic acid steam reforming. 16th International Conference on Clean Energy.

[19] Ali Bashah, N. A., Luin, A., Jalaluddin, I. A., Shahhaizad, I. A., Ismail, N. F. and Wan Kamis. W. Z. (2019). Characteristics of chromium based mixed oxide catalyst in biodiesel production. Journal of Physics: Conference Series, 1349: 012143.

[20] Cuesta Zapata, P. M., Nazzarro, M. S., Parentis, M. L., Gonzo, E. E. and Bonini, N. A. (2013). Effect of hydrothermal treatment on Cr-SiO_2 mesoporous materials. Chemical Engineering Science, 101: 374-381.

[21] Turek, W., Haber, J. and Krowiak, A. (2005). Dehydration of isopropyl alcohol used as an indicator of the type and strength of catalyst acid centres. Applied Surface Science, 252: 823–827.

[22] Chen, X., Shen, Y. F., Suib, S. L. and O'Young, C. L. (2001). Catalytic decomposition of 2-propanol over different metal-cation-doped OMS-2 materials. Journal of Catalysis, 197: 292–302.

[23] Fahim, R. B., Zaki, M. I. and Gabr, R. M. (1982). The catalytic decomposition of 2-propanol on calcined chromia: the nature of the active sites. Applied Catalysis, 4: 189-200.

[24] Richter, M. and Öhlmann, G. (1985). Influence of Cr loading on the catalytic properties of CrO_3/SiO_2 catalyts in 2-propanol conversion. Reaction Kinetics and Catalysis Letters, 29: 211-218.

[25] Ilyas, M., Shah, S., Nigar, R. and Khan, H. (1994). Conversion of lsopropyl Alcohol to Acetone Catalysed by Cr_2O_3 at 473 K: Role of Molecular Oxygen. Journal of the Chemical Society, Faraday Transactions, 90: 2413-2415.

[26] Bautista, F. M., Campelo, J. M., Garcia, A., Luna, D., Marinas, J., Romero, A. A. and Urbano, M. R. (1995). Conversion of 2-propanol over chromium aluminum orthophosphates. Catalysis Letters, 35: 143-154.

[27] Trejda, M., Wojtaszek, A., Ziolek, M. and Kujawa, J. (2009). Various hexagonally ordered mesoporous silicas as supports for chromium species—The effect of support on surface properties. Applied Catalysis A: General, 365: 135–140.

[28] Wang, Y., Ohishi, Y., Shishido, T., Zhang, Q., Yang, W., Guo, Q., Wan, H. and Takehira, K. J. (2003). Characterizations and catalytic properties of Cr-MCM-41 prepared by direct hydrothermal synthesis and template-ion exchange. Journal of Catalysis, 220: 347–357.

[29] Gómez-Cazalilla, M., Mérida-Robles, J. M., Gurbani, A., Rodríguez-Castellón, E. and Jiménez-López, A. (2007). Characterization and acidic properties of Al-SBA-15 materials prepared by post-synthesis alumination of a low-cost ordered mesoporous silica. Journal of Solid State Chemistry, 180: 1130–1140.

[30] Mimura, N., Okamoto, M., Yamashita, H., S. T. Oyama, S. T. and Murata, K. (2006). Oxidative Dehydrogenation of Ethane over Cr/ZSM-5 Catalysts Using CO_2 as an Oxidant. The Journal of Physical Chemistry B, 110 (43): 21764-21770.

[31] Shupack, S. I (1991). The Chemistry of Chromium and Some Resulting Analytical Problems. Environmental Health Perspectives, 92: 7-11.

[32] Wang, G., Zhang, L., Deng, J., Dai, H., He, H. and Au, C. T. (2009). Preparation, characterization, and catalytic activity of chromia supported on SBA-15 for the oxidative dehydrogenation of isobutene. Applied Catalysis A: General, 355: 192–201.

[33] Zhang, L., Zhao, Y., Dai, H., He, H. and C. T. Au, C. T. (2008). A comparative investigation on the properties of Cr-SBA-15 and CrOx/SBA-15. Catalysis Today, 131: 42–54.

[34] Liu, Y. M., Cao, Y., Yi, N., Feng, W. L., Dai, W. L., Yan, S. R., He, H. Y. and Fan, K. N. (2004). Vanadium oxide supported on mesoporous SBA-15 as highly selective catalysts in the oxidative dehydrogenation of propane. Journal of Catalysis, 224, 417–428.

[35] Kumar, M. S., Hammer, N., Rønning, M., Holmen, A., Chen, D., Walmsley, J. C. and G. Øye, G. (2009). The nature of active chromium species in Cr-catalysts for dehydrogenation of propane: New insights by a comprehensive spectroscopic study. Journal of Catalysis, 261: 116–128.

[36] Zhao, D., Feng, J., Huo, V. Q., Melosh, N., Fredrickson, G. H., Chmelka, B. F. and G. D. Stucky. (1998). Triblock copolymer syntheses of mesoporous silica with periodic 50 to 300 angstrom pores. Science, 279, 548-552.

[37] Charan, P. H. K. and G. R. Rao, G. R. (2015). Textural and morphological studies of transition metal doped SBA-15 by co-condensation method. Journal of Chemical Sciences, 127: 909-919.

[38] Liu, H., Li, Y., Wu, H., Takayama, H., Miyake, T. and He, D. (2012). Effects of β-cyclodextrin modification on properties of Ni/SBA-15 and its catalytic performance in carbon dioxide reforming of methane. Catalysis Communications, 28: 168-173.

[39] McMurdie H., Morris, M., Evans, E., Paertzkin, B.,Ng-Wong, W., Zhang, Y. and C. R. Hubbard, C. R. (1987). Standard X-ray diffraction powder patterns from the JCPDS research associateship, Power Diffraction, 2: 41–52.

[40] Gómez-Cazalilla, M., Infantes-Molina, A., Moreno-Tost, R., Maireles-Torres, P. J. Mérida-Robles, J., Rodríguez-Castellón, E. and Jiménez-López, A. (2009). Al-SBA-15 as a support of catalysts based on chromium sulfide for sulfur removal. Catalysis Today, 143: 137–144.

[41] Basaldella, E. I., Tara, J. C., Aguilar, Armenta, G. and Patiño, Iglesias, M. E. (2007). Cu/SBA-15 as adsorbent for propane/propylene separation. Journal of Porous Materials, 14: 273-278.

[42] Gregg, S. L. and Sing, K. S. W. (1982). Adsorption, Surface Area and Porosity, 2nd edn., Academic Press INC, London, pp. 233-234.

[43] Marcus, Y. (1983). Ionic radii in aqueous solutions. Journal of Solution Chemistry, 12: 271-275.

[44] Fouad, N. E. (2000). Formation of Cr (II) species in the H_2/CrO_3 system. Journal of Thermal Analysis and Calorimetry, 60: 541–547.

[45] Cavani, F., Koutyrev, M., Trifiro, F., Bartolini, A., Ghisletti, D., Iezzi, R., Santucci, A. (1996). Chemical and physical characterization of alumina-supported chromia-based catalysts and their activity in dehydrogenation of isobutane. Journal of Catalysis, 158, 236–250.

[46] Nondek, L. and Sedláček, J. (1975). Mechanism of dehydrogenation of secondary alcohols on chromia. Journal of Catalysis, 40: 34-39.

[47] Ogonowski, J. and Skrzyńska, E. (2008). Deactivation of VMgOx catalysts by coke in the process of isobutane dehydrogenation with carbon dioxide. Catalysis Letters, 121: 234-240.

[48] Marakami, Y., Sawata, A. and Tsuru, Y. (1999). Crystallization behavior of amorphous solid solutions and phase separation in the Cr_2O_3-Fe_2O_3 system. Journal of Materials Science, 34, 951-955.

[49] Fang, D., Zhao, J., Li, W., Fang, X., Yang, X., Ren, W. and Zhang, H. (2015). Investigation of the characteristics and deactivation of catalytic active center of Cr-Al_2O_3 catalysts for isobutane dehydrogenation. Journal of Energy Chemistry, 24 (1): 101-107.

[50] Weckhuysen, B. M, Verberckmoes, A. A., De Baets, A. R. and Schoonheydt, R. A. (1997). Diffuse reflectance spectroscopy of supported chromium oxide catalysts: A self-modeling mixture analysis. Journal of Catalysis, 166: 160-171.

[51] Yamashita, H., Yoshizawa, K., Ariyuki, M., Higashimoto, S., M., Che, M. and Anpo, M. (2001). Photocatalytic reactions on chromium containing mesoporous silica molecular sieves (Cr-HMS) under visible light irradiation: decomposition of NO and partial oxidation of propane. Chemical Communications, 435-436.

[52] Nijhuis, T. A. Tinnemans, S. T., Visser, T. and B. M. Weckhuysen, B. M. (2004). Towards real-time spectroscopic process control for the dehydrogenation of propane over supported chromium oxide catalysts. Chemical Engineering Science, 59: 5487-5492.

[53] Weckhuysen, B. M., De Ridder, L. M. and R. A. Schoonheydt. R. A. (1993). A Quantitative Diffuse Reflectance Spectroscopy Study of Supported Chromium Catalysts. The Journal of Physical Chemistry, 97: 4756-4763.

[54] Botavina, M. A., Agafonov, Y. A., Gaidai, N. A., Groppo, E., Cortés Corberán, V., Lapidus, A. L. and Martra, G. (2016). Towards efficient catalysts for the oxidative dehydrogenation of propane in the presence of CO_2: Cr/SiO_2 systems prepared by direct hydrothermal synthesis. Catalysis Science & Technology, 6: 840-850.

[55] Silverstein, R. M., Webster F. X., Spectrometric Identification of Organic Compounds, 6rd ed., New York: John Wiley & Sons, Inc. 1998, pp 90, 108, 140.

[56] Wang, Y., Ren, J., Liu, X., Wang, Y., Guo, Y., Guo, Y., & Lu, G. (2008). Facile synthesis of ordered magnetic mesoporous γ-Fe_2O_3/SiO_2 nanocomposites with diverse mesostructures. Journal of Colloid and Interface Science, 326 (1), 158-165.

[57] Tsoncheva, T., Roggenbuck, J., Paneva, D., Dimitrov, M., Mitov, I., & Fröba, M. (2010). Nanosized iron and chromium oxides supported on mesoporous CeO_2 and SBA-15 silica: Physicochemical and catalytic study. Applied Surface Science, 257 (2), 523-530.

[58] Trejda, M., Bryś, M., & Ziolek, M. (2014). Relationship between basicity, reducibility and partial oxidation properties of chromium containing MCM-41. RSC Advances, 4 (108), 62940-62946.